D and Q-axes Inductance Estimation and Self-Sensing Condition Monitoring using 45° angle High-Frequency Injection

Ye gu Kang, *Member, IEEE,* David Reigosa, *Member, IEEE,* Bulent Sarlioglu, *Senior Member, IEEE*
Robert D. Lorenz, *Fellow, IEEE*

***Abstract*—This paper proposes a high-frequency injection (HFI) based dq-inductance estimation technique for synchronous machines. The d and q-axes inductance are estimated using a single HF injection between dq-axes, i.e., 45° injection angle. The d and q-axes incremental inductance variation over four quadrants dq-plane operating condition is evaluated. The proposed technique can operate in real-time without a controlled position or velocity from the load side. No previous knowledge of machine parameters nor computationally expensive regression processes are required. The proposed technique can be used to evaluate the sensitivity of inductive-saliency based self-sensing to determine preferable self-sensing operating conditions for permanent magnet synchronous machines (PMSMs).**

***Index Terms*—High-frequency injection (HFI), Incremental inductance estimation, Surface permanent magnet synchronous machine (SPMSM)**

NOMENCLATURE

I_{ch}	Characteristic current.
λ_{PM}	Permanent magnet flux linkage.
t_{PM}	Permanent magnet temperature.
$\lambda_{qs}^{\theta_r}, \lambda_{ds}^{\theta_r}$	Stator q- and d-axes flux linkages in the rotor reference frame.
θ_r	Rotor angular position.
$\hat{\theta}_r$	Estimated rotor angular position.
i_{qs}^{s}, i_{ds}^{s}	Stator q- and d-axes current in the stator reference frame.
$i_{qsHF}^{\theta_r}, i_{dsHF}^{\theta_r}$	Stator q- and d-axes high-frequency current in the rotor reference frame.
$i_{qs}^{\hat{\theta}_r}, i_{ds}^{\hat{\theta}_r}$	Stator q- and d-axes current in the estimated rotor reference frame.
$v_{qsHF}^{\theta_r}, v_{dsHF}^{\theta_r}$	Stator q- and d-axes high-frequency voltage input in the rotor reference frame.
$L_{inc.}, L_{abs.}$	Incremental and absolute inductance.
L_q, L_d	Absolute q- and d-axes inductance.
L_{qq}, L_{dd}	Incremental q- and d-axes inductance.
$\Sigma L, \Delta L$	Average and differential inductance.
R_q, R_d	Q- and d-axes resistance.
I_{i0}, I_{i1}	Average and differential current.
V_{HFI}	High-frequency injection voltage.
f_{HFI}	High-frequency injection frequency.
FI	Flux-intensifying.
FW	Flux-weakening.
LPF	Low pass filter.
PI	Proportional and integral controller.
PM	Permanent magnet.
PWM	Pulse width modulation.
VSI	Voltage source inverter.

I. INTRODUCTION

Accurate estimation of the inductance in permanent magnet synchronous machines (PMSMs) is critical for estimating the machine states, e.g. back-EMF [1], [2], High frequency (HF) current [3], [4], flux [5], [6], torque [7], and PM temperature [8], [9]. The estimation accuracy of machine states often depends on inductance parameter accuracy; e.g. the back-EMF [1], [2], HF current [3], [4], or flux [5], [6] states estimation. These states estimation, classically using observers or state filters, depends on the machine inductances, which varies due to machine normal operation, e.g., due to the saturation induced by armature current injection or PM temperature [8]–[10]. Inductance estimation is therefore critical for machine model-based states estimation, e.g., torque [7] or PM temperature estimation [8], [9].

Inductance estimation techniques can be roughly classified into: off-line [10]–[18] and on-line [19]–[26] estimation techniques. Off-line estimation techniques can be further divided into locked rotor [10]–[12], constant speed [13], [14] and free-wheeling [15]–[18] estimation techniques; all of them considering saturation and cross saturation effects. Both locked rotor [10]–[12], and constant speed [13], [14] off-line estimation techniques require position/velocity to be controlled from load machine and additional driver linked to the test machine. To overcome this limitation, free-wheeling test techniques have been proposed [15]–[18]. These techniques require a regression process, which needs data set from multiple tests to result in accurate inductance estimation; completing the off-line inductance estimation, inductance variations could be stored in look-up tables, or curve fit equations [27], [28]. It is noted that the accuracy of the look-up table is only valid within the pre-commissioned operating conditions. Finally, it is noted that PM temperature changes during normal machine operation, being a parameter difficult to measure/estimate [10], [29]. For this reason, PM temperature, which affects d-axis magnetic loading and, therefore, inductance, is often omitted in the evaluation process.

On-line estimation techniques can be divided into: model reference adaptive systems (MRASs) [19]–[22] or HF injection based techniques [23]–[26]. MRAS schemes are widely employed due to their relative simplicity and low computational effort [19]–[22]. MRAS techniques are closed-loop processes, which require an error vector formed from the output of two models, both dependent on different motor parameters; the target parameter estimation accuracy, in this case, inductance, depending therefore on machine parameters accuracy (e.g., resistance, back-EMF, dq-transform induced coupled voltage). For these reasons, MRAS cannot adjust the model fast enough in dynamic load conditions [22]. To overcome the aforementioned limitations, HF injection-based methods have been proposed [23]–[26]. By Using a HF signal superimposed on the fundamental excitation, machine inductance can be estimated online and in all operating speed, including stand still. The HFI based inductance estimation techniques requires to inject more than two HF signals separately to estimate d and q-axes inductance, [23], [24]. The inductance estimation accuracy is dependent on the error angle between the estimation angle from HFI self-sensing and position sensor angle [25], [26]. While these HFI techniques estimate the dq-inductance, they are not developed to monitor self-sensing ability.

This paper focuses on dq-inductance estimation and inductive saliency based self-sensing condition monitoring using HFI. In machines with inductive saliency, the rotor position can be estimated by using HFI [4], [30]–[34]. Conversely, given the rotor position, incremental dq-inductance can be estimated using HFI. The proposed inductance estimation technique is based on injecting an HF signal at 45°, i.e., in between d and q-axes [35]. The proposed technique does not require pre-commissioning processes nor the machine model. It will be shown that by injecting an HF voltage in between d and q-axes, the average and differential HF current are automatically decoupled, allowing both d and q-axes inductance estimation with only one HF signal injection, and in real-time. The proposed technique enables, therefore, real-time inductance estimation in any operating condition and can be further used for self-sensing sensitivity monitoring purposes.

Table I summarizes the existing inductance estimation techniques. Off-line based techniques share common characteristics of open-loop algorithms, i.e., they need pre-commissioning processes requiring load-side position or velocity control or requiring heavy regression processes. Also, off-line based techniques do not have disturbance rejection capabilities. On the other hand, on-line based techniques share characteristics of closed-loop algorithms, i.e., they have disturbance rejection capability in real-time. MRAS based methods have the limitation of requiting previous knowledge of machine parameters, while HFI based techniques have the drawback of requiring the injection of a small-magnitude HF signal, however, they don't require previous knowledge of machine parameters nor computationally expensive regression process.

The proposed HFI method has advantage among the other HFI estimation algorithm in computational efficiency. The number of filters and computation are reduced by half compared to the other HFI based inductance estimation methods since the proposed method uses a single signal injection at 45°. The proposed HFI method will be shown to result in a simpler implementation (only one HF signal will be required); in addition, it can be used for self-sensing sensitivity monitoring function. The inductive saliency variation, caused by nonlinear effects, change the performance of the HFI based self-sensing [30]–[34]. The decoupled differential HF current, I_{i1}, will be used for evaluating the self-sensing ability of PMSMs to find preferable operating conditions from the self-sensing point of perspective. The proposed technique will be evaluated on surface PMSMs; the four dq-current operating quadrants will be evaluated, see Fig. 1.

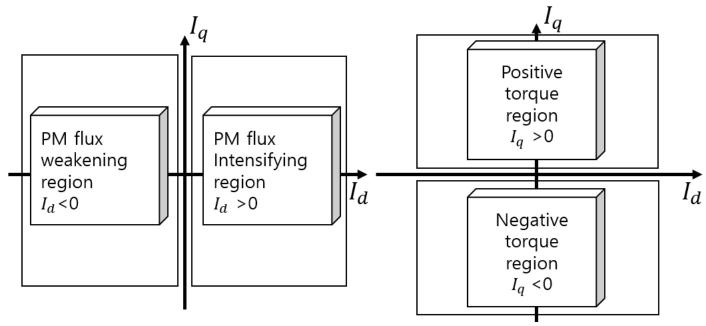

Fig. 1: SPMSM operating condition in dq-current quadrants.

The paper is organized as follows: PMSMs dq-inductance model is presented in section II; section III shows the HFI based incremental inductance estimation technique; experimental results are shown in section IV; conclusions are provided in section V.

II. Dq-inductance model in PMSMs

This section presents the inductance model of PMSMs, including magnetic saturation conditions.

The absolute and incremental flux model in (1) and (2) are function of dq-current, $i_{ds}^{\theta_r}$, $i_{qs}^{\theta_r}$, and PM temperature, t_{PM} where L_q and L_d are the absolute inductance and L_{qq} and L_{dd} are the incremental inductance. The cross saturation in (1) and (2) is represented by making the dq-inductance function of both dq-current. The strength of the flux generated by PM is a function magnet temperature, t_{PM}, and included in the inductance model.

Figure 2 shows the absolute and incremental inductance definitions [36], [37]. The absolute inductance, $L_{abs.}$, at point b, represents the total amount of induced flux linkage, λ_0, for a fundamental current level, I_0. The absolute inductance represents the fundamental flux component to produce torque, which is commonly used in controller tuning, axes decoupling, or to define the maximum torque per ampere (MTPA) trajectory [10]. The incremental inductance, $L_{inc.}$ in between point b and c represents the incremental flux linkage, $\Delta\lambda$, with incremental current, ΔI_0. The incremental inductance is used in high frequency and small-signal injection-based self-sensing or state estimation algorithms [4], [7], [29].

$$\begin{bmatrix}\lambda_{qs}^{\theta_r}\\ \lambda_{ds}^{\theta_r}\end{bmatrix} = \begin{bmatrix}L_q(i_{qs}^{\theta_r}, i_{ds}^{\theta_r}, t_{PM}) & 0\\ 0 & L_d(i_{qs}^{\theta_r}, i_{ds}^{\theta_r}, t_{PM})\end{bmatrix}\begin{bmatrix}i_{qs}^{\theta_r}\\ i_{ds}^{\theta_r}\end{bmatrix} + \begin{bmatrix}0\\ \lambda_{PM}(t_{PM})\end{bmatrix} \tag{1}$$

TABLE I: Inductance estimation techniques comparison

	Off-line			On-line			
	Locked rotor [10]–[12]	Constant speed [13], [14]	Free wheeling [15]–[18]	MRAS [19]–[22]	HFI: Two signals [23], [24]	HFI: Injection error [25], [26]	HFI: 45°(Proposed) [35]
Require other machine parameters	Yes	Yes	Yes	Yes	No	No	No
Load side control required	Yes[1]	Yes	No	No	No	No	No
Regression process required	Yes	Yes	Yes[2]	No	No	No	No
Disturbance rejection	No	No	No	Yes	Yes	Yes	Yes
Interference during operation	No	No	No	No	Yes	Yes	Yes
Real-time estimation	No	No	No	Yes[3]	Yes	Yes	Yes
Computationally efficient	No	No	No	No	No[4]	Yes	Yes
Self-sensing sensitivity monitoring	No	No	No	No	No	No	Yes

[1]Rotor position must be fixed in a position during commissioning process.
[2]Data set required from multiple test.
[3]Slow in estimation in transient condition.
[4]The number of filter and computation increases with the number of injected signals.

$$\begin{bmatrix}\Delta\lambda_{qs}^{\theta_r}\\ \Delta\lambda_{ds}^{\theta_r}\end{bmatrix} = \begin{bmatrix}L_{qq}(i_{qs}^{\theta_r}, i_{ds}^{\theta_r}, t_{PM}) & 0\\ 0 & L_{dd}(i_{qs}^{\theta_r}, i_{ds}^{\theta_r}, t_{PM})\end{bmatrix}\begin{bmatrix}\Delta i_{qs}^{\theta_r}\\ \Delta i_{ds}^{\theta_r}\end{bmatrix} \quad (2)$$

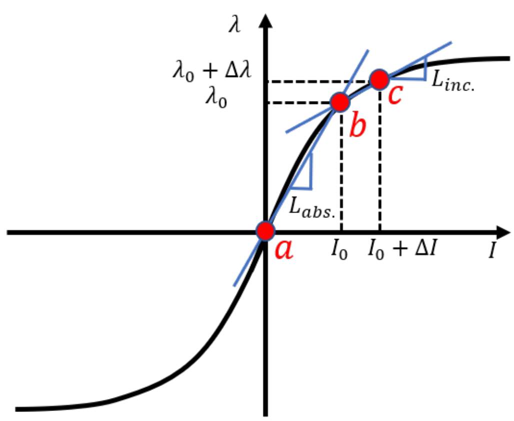

Fig. 2: Incremental and absolute inductance.

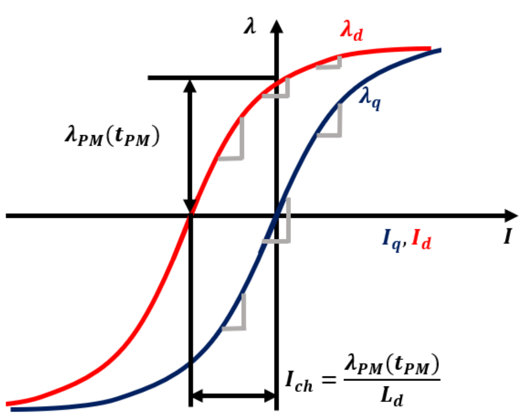

Fig. 3: SPMSM dq-flux linkage Vs. armature current including saturation effect.

Figure 3 shows the dq-flux linkage as function of the dq-current for SPMSMs including saturation effect. Since the rotor and the stator of SPMSMs are symmetrically designed, the only difference between d and q-axes is the magnetic loading from the PM flux. Note that the d-axis flux path is biased by the PM flux linkage, λ_{PM}, i.e., the d-axis flux linkage is horizontally shifted to the left. Characteristic current, I_{ch}, will be required to set the q-axis saturation level at the initial d-axis saturation level.

From Fig. 2 and Fig. 3, following conclusions can be made:

- Incremental inductance can be estimated only by injecting small Δi superimposed on top of the fundamental current component.
- SPMSMs have inductive saliency due to magnetic saturation. D and q-axes magnetic circuit are asymmetric since PM flux source is aligned with the d-axis.
- The d and q-axes inductance deviation from the nominal values is a reliable metric of magnetic saturation level on each axis.
- The d-axis incremental inductance tends to decrease in flux-intensifying (FI) operation, i.e., +I_d, and increase in flux-weakening (FW) operation, i.e., -I_d.

III. HFI based Incremental Inductance Estimation

This section presents the proposed dq-inductance estimation and self-sensing monitoring technique.

A. HF model in arbitrary reference frame

Equation (3) shows the fundamental model of a SPMSM in the synchronous reference frame, where $v_{qs}^{\theta_r}$, $v_{ds}^{\theta_r}$, $\lambda_{qs}^{\theta_r}$, $\lambda_{ds}^{\theta_r}$, and $i_{qs}^{\theta_r}$, $i_{ds}^{\theta_r}$ are the q- and d-axes voltage, flux linkage, and current in the synchronous reference frame, R_q, R_d, are the q- and d-axes resistance, ω_r is the rotor angular velocity, and p is the time derivative operator. The q and d-axes flux linkages are defined by (1).

$$\begin{bmatrix}v_{qs}^{\theta_r}\\ v_{ds}^{\theta_r}\end{bmatrix} = \begin{bmatrix}R_q & 0\\ 0 & R_d\end{bmatrix}\begin{bmatrix}i_{qs}^{\theta_r}\\ i_{ds}^{\theta_r}\end{bmatrix} + p\begin{bmatrix}\lambda_{qs}^{\theta_r}\\ \lambda_{ds}^{\theta_r}\end{bmatrix} + \omega_r\begin{bmatrix}\lambda_{ds}^{\theta_r}\\ -\lambda_{qs}^{\theta_r}\end{bmatrix} \quad (3)$$

When a high-frequency signal is injected, and assuming the the resistance term can be safely neglected as the inductance dominates on the machine impedance and that the cross-coupling flux linkage effect can be safely neglected (i.e. the HF injection frequency is much higher than the ω_r), the resulting HF voltage equation is shown in (4); which is obtained from (2) and (3). Note that the dq-inductances are function of the fundamental current in dq reference frame. For further development, $(i_{qs}^{\theta_r}, i_{ds}^{\theta_r}, t_{PM})$ are skipped.

$$\begin{bmatrix} v_{qsHF}^{\theta_r} \\ v_{dsHF}^{\theta_r} \end{bmatrix} = p \begin{bmatrix} L_{qq}(i_{qs}^{\theta_r}, i_{ds}^{\theta_r}, t_{PM}) & 0 \\ 0 & L_{dd}(i_{qs}^{\theta_r}, i_{ds}^{\theta_r}, t_{PM}) \end{bmatrix} \begin{bmatrix} i_{qsHF}^{\theta_r} \\ i_{dsHF}^{\theta_r} \end{bmatrix} \tag{4}$$

(4) can be expressed in an arbitrary reference frame as (7), where (5) is the Park transform, (6), is the injection angle, θ_r is the rotor electrical position, and θ_{offset} is the HF injection offset angle as shown in Fig. 4; The resulting HF model being (8) where the differential inductance, ΔL, and the average inductance, ΣL, are defined by (9) and (10) respectively.

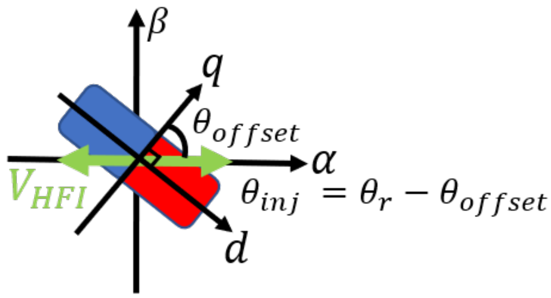

Fig. 4: Pulsating voltage injection angle with offset angle.

$$K_p = \begin{bmatrix} \cos(\theta_{inj}) & \sin(\theta_{inj}) \\ -\sin(\theta_{inj}) & \cos(\theta_{inj}) \end{bmatrix} \tag{5}$$

$$\theta_{inj} = \theta_r - \theta_{offset} \tag{6}$$

$$K_p \begin{bmatrix} i_{qsHF}^{\theta_r} \\ i_{dsHF}^{\theta_r} \end{bmatrix} = \{K_p \begin{bmatrix} L_{qq} & 0 \\ 0 & L_{dd} \end{bmatrix}^{-1} K_p^{-1}\}\{\frac{1}{p} K_p \begin{bmatrix} v_{qsHF}^{\theta_r} \\ v_{dsHF}^{\theta_r} \end{bmatrix}\} \tag{7}$$

$$\begin{bmatrix} i_{qsHF}^{\theta_{inj}} \\ i_{dsHF}^{\theta_{inj}} \end{bmatrix} = \frac{1}{(\Sigma L^2 - \Delta L^2)} \begin{bmatrix} \Sigma L + \Delta L\cos(2\theta_{inj}) & -\Delta L\sin(2\theta_{inj}) \\ -\Delta L\sin(2\theta_{inj}) & \Sigma L - \Delta L\cos(2\theta_{inj}) \end{bmatrix} \frac{1}{p} \begin{bmatrix} v_{qsHF}^{\theta_{inj}} \\ v_{dsHF}^{\theta_{inj}} \end{bmatrix} \tag{8}$$

$$\Delta L = \frac{L_{qq} - L_{dd}}{2} \tag{9}$$

$$\Sigma L = \frac{L_{qq} + L_{dd}}{2} \tag{10}$$

B. HFI dq-inductance estimation with Pulsating voltage in 45° angle

If θ_{inj} is fixed to $-45°$ (11), and the rotor position is measured by a position sensor, e.g. with an encoder, and a pulsating HF voltage is injected (12), the resulting HF current can be defined by (13), where V_{HFI} is the HF injection voltage magnitude, f_{HFI} is the HF injection frequency, I_{i0} is the average HF current magnitude, and I_{i1} is the differential HF currents magnitude; I_{i0} and I_{i1} are defined by (14). It can be observed from (13) and (14) that the average and differential HF current are decoupled from each other. As a result, d and q-axes HF inductance can be estimated from (15) and (16).

$$\theta_{inj} = -45° \tag{11}$$

$$\begin{bmatrix} v_{qsHF}^{\theta_{inj}} \\ v_{dsHF}^{\theta_{inj}} \end{bmatrix} = V_{HFI}\cos(2\pi f_{HFI} t) \begin{bmatrix} 1 \\ 0 \end{bmatrix} \tag{12}$$

$$\begin{bmatrix} i_{qsHF}^{\theta_{inj}} \\ i_{dsHF}^{\theta_{inj}} \end{bmatrix} = \sin(2\pi f_{HFI} t) \begin{bmatrix} I_{i0} \\ I_{i1} \end{bmatrix} \tag{13}$$

$$\begin{bmatrix} I_{i0} \\ I_{i1} \end{bmatrix} = \frac{V_{HFI}}{2\pi f_{HFI}(\Sigma L^2 - \Delta L^2)} \begin{bmatrix} \Sigma L \\ \Delta L \end{bmatrix} \tag{14}$$

$$\hat{L}_{qq} = \frac{V_{HFI}}{2\pi f_{HFI}(I_{i0} - I_{i1})} \tag{15}$$

$$\hat{L}_{dd} = \frac{V_{HFI}}{2\pi f_{HFI}(I_{i0} + I_{i1})} \tag{16}$$

It can be observed that dq-inductance estimation becomes rather simplified when injecting the HF signal in between dq-axes, i.e., θ_{inj} being $-45°$. When the injection angle is not fixed to $-45°$, the average and differential HF current will be coupled, as shown in (17). The inductance estimation error will occur in case of an error in the injection angle as shown by (18) and (19). This error in the injection angle could due to the position sensor, e.g. an encoder, resolution. The corresponding maximum angle error and resulting dq-inductance estimation error for 8, 10, and 12-bit incremental encoder is summarized in Table II for a 4 pole pair machine and $I_{i1} = 0.1 I_{i0}$. The maximum inductance estimation error using a 12 bit encoder position error is less than 1%.

$$\begin{bmatrix} i_{qsHF}^{\theta_{inj}} \\ i_{dsHF}^{\theta_{inj}} \end{bmatrix} = \sin(2\pi f_{HFI} t) \begin{bmatrix} I_{i0} + I_{i1}\cos(2\theta_{inj}) \\ -I_{i1}\sin(2\theta_{inj}) \end{bmatrix} \tag{17}$$

$$\hat{L}'_{qq} = \frac{V_{HFI}}{2\pi f_{HFI}(I_{i0} + I_{i1}\cos(2\theta_{inj}) + I_{i1}\sin(2\theta_{inj}))} \tag{18}$$

$$\hat{L}'_{dd} = \frac{V_{HFI}}{2\pi f_{HFI}(I_{i0} + I_{i1}\cos(2\theta_{inj}) - I_{i1}\sin(2\theta_{inj}))} \tag{19}$$

TABLE II: Inductance estimation error due to position error

# of bit encoder	Max. mech. angle error [deg.]	Max. elec. angle error[1] [deg.]	Max. $\hat{L}_{qq}$ error[2] [%]	Max. $\hat{L}_{dd}$ error[2] [%]
8	1.41	5.63	2.45	1.64
10	0.35	1.41	0.59	0.45
12	0.088	0.35	0.14	0.12

[1] 4 pole pair is used.
[2] $I_{i1} = 0.1 I_{i0}$ is used.

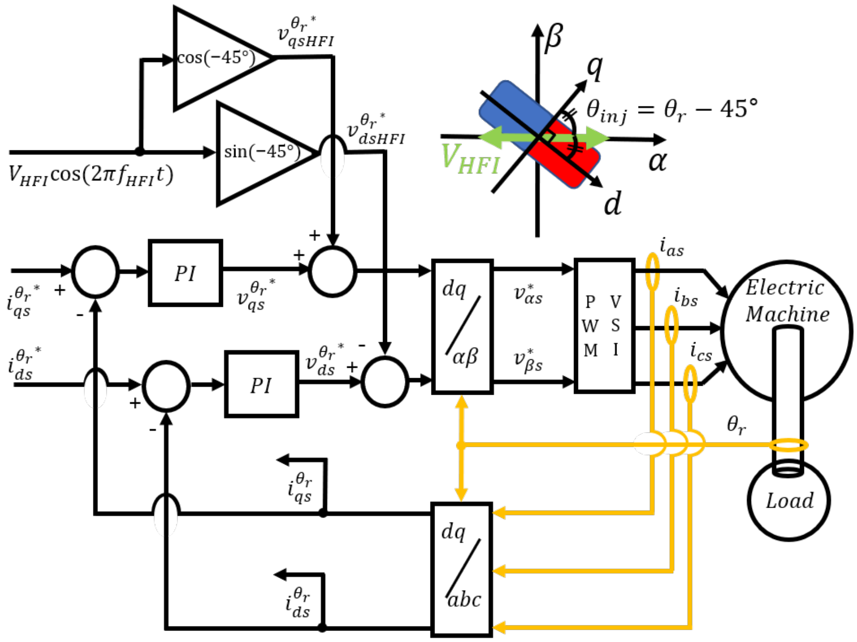

Fig. 5: Saturation monitoring system block diagram.

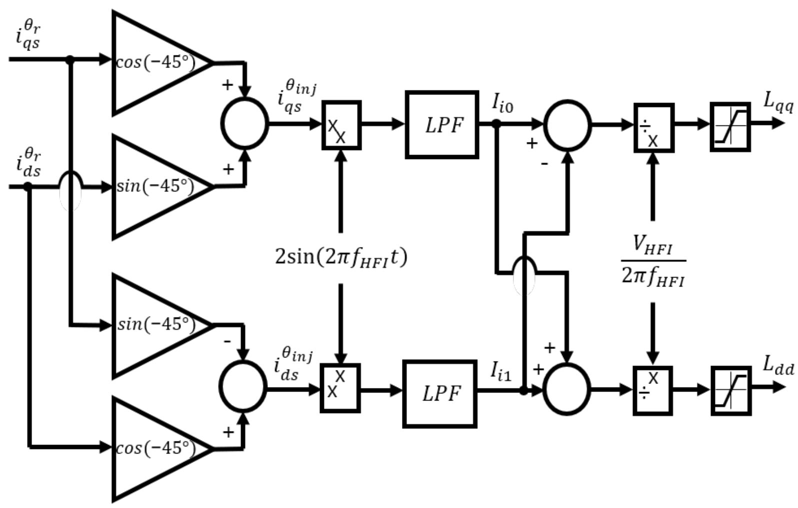

Fig. 6: Incremental inductance estimation block diagram.

C. *HFI self-sensing ability monitoring*

HFI based self-sensing is based on the inductive saliency. When q-axis pulsating HF voltage (20) is injected in the estimated reference frame, (7) becomes (21), where θ_{error} is defined in (22). Equation (21) can be rewritten in terms of the deferential and average current as (23). Note that the I_{i0} and I_{i1} consist of the average and differential inductance which are function of dq-current and magnet temperature. This is due to saturation effect shown in (2). The position estimation using HFI is typically done by nullifying control $i_{dsHF}^{\hat{\theta}_r}$ in (23) that is function of I_{i1} and the position estimation error, θ_{error}. It can be observed that by increasing I_{i1}, the HF current error due to position estimation error, θ_{error}, increases. Thus, the sensitivity of the d-axis HF current in the estimated rotor reference frame with respect to θ_{error} is determined by the magnitude of the differential current, I_{i1}, which varies under magnetic saturation. Note that the I_{i1} is function of L_{dd} and L_{qq} as well as HF injection voltage and frequency. It can be therefore concluded from the previous discussion that self-sensing sensitivity can be improved by increasing V_{HFI} and decreasing f_{HFI}. In closed-loop self-sensing control, the magnitude of I_{i1} is difficult to be evaluated because $i_{dsHF}^{\hat{\theta}_r}$ is nullifying controlled for zero position estimation error, θ_{error}. To decouple I_{i1} from the estimated position error, a pulsating voltage injection injected in $-45°$ can be used as was stated in the previous section. The decoupled differential HF current, I_{i1}, can be therefore used to evaluate the self-sensing ability of PMSMs to find preferable operating conditions.

$$\begin{bmatrix} v_{qsHF}^{\hat{\theta}_r} \\ v_{dsHF}^{\hat{\theta}_r} \end{bmatrix} = V_{HFI}\cos(2\pi f_{HFI}t)\begin{bmatrix} 1 \\ 0 \end{bmatrix} \tag{20}$$

$$\begin{bmatrix} i_{qsHF}^{\hat{\theta}_r} \\ i_{dsHF}^{\hat{\theta}_r} \end{bmatrix} = \frac{V_{HFI}\sin(2\pi f_{HFI}t)}{2\pi f_{HFI}(\Sigma L^2 - \Delta L)} \begin{bmatrix} \Sigma L + \Delta L\cos(2\theta_{error}) \\ -\Delta L\sin(2\theta_{error}) \end{bmatrix} \quad (21)$$

$$\theta_{error} = \theta_r - \hat{\theta}_r \quad (22)$$

$$\begin{bmatrix} i_{qsHF}^{\hat{\theta}_r} \\ i_{dsHF}^{\hat{\theta}_r} \end{bmatrix} = \sin(2\pi f_{HFI}t) \begin{bmatrix} I_{i0}(i_{qs}^{\theta_r}, i_{ds}^{\theta_r}, t_{PM}) + I_{i1}(i_{qs}^{\theta_r}, i_{ds}^{\theta_r}, t_{PM})\cos(2\theta_{error}) \\ -I_{i1}(i_{qs}^{\theta_r}, i_{ds}^{\theta_r}, t_{PM})\sin(2\theta_{error}) \end{bmatrix} \quad (23)$$

IV. Experiment

This section presents the experimental results of the proposed incremental inductance estimation technique. The inductance monitoring system block diagram is shown in Fig. 5. The HF is injected at $-45°$ of the rotor reference frame. The machine can operate in any condition, i.e., dq-current, PM temperature, velocity. The post-processing for estimation of incremental inductance is shown in Fig. 6. The three phase current is transformed to the injection reference frame to result in decoupled I_{i0}, and I_{i1}. The HF current are then used for estimation of the dq- incremental inductance in real-time.

TABLE III: Test SPMSMs Parameters

	DW SPMSM	DW SPMSM	FSCW SPMSM
Model	Cumstom made	Teknic-M2310P	CMC-T0603P0105
# poles	8	8	8
# slots	24	12	18
I_{rated} [A]	15	7	6
R_p [Ω]	0.1	0.377	0.386
L_p [mH]	7.5	0.24	0.67

This section is subdivided into two subsections: The first subsection will show the inductance estimation result on the four-quadrant operating condition for a distributed winding (DW) SPMSM. The second subsection will compare the incremental inductance variation for a DW-SPMSM, and a fractional-slot concentrated winding (FSCW) SPMSMs. The parameters of both test SPMSMs are shown in Table III and Fig.7.

A. Incremental dq-inductance estimation using 45° injection angle

Figure 7 (a) shows an 8-pole 24-slot DW SPMSM, which is loaded with an axial PMSM driven by a BAMOCAR-PG-D3 power converter. Figure 8 shows an example of the real-time inductance estimation. Figure 8 (a) shows the measured stator d and q-axes currents in the rotor reference frame. Figure 8 (b) shows the average and the differential HF current, I_{i0} and I_{i1}, using the signal processing shown in Fig. 6, second-order low pass filter with cutoff frequency of 100Hz has

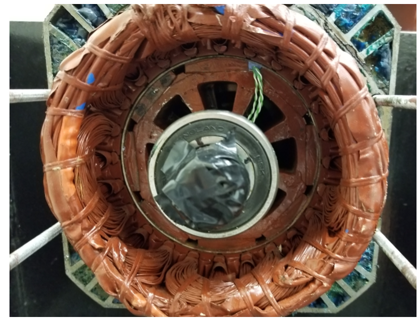

(a) 8-pole, 24-slot SPMSM.

(b) 8-pole, 12-slot SPMSM.

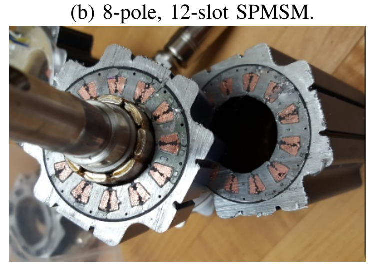

(c) 8-pole, 18-slot SPMSM.

Fig. 7: Test SPMSMs.

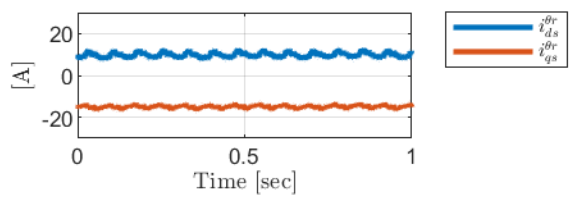

(a) Stator dq current in rotor reference frame.

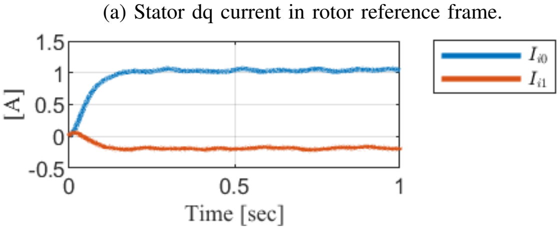

(b) Average and differential current.

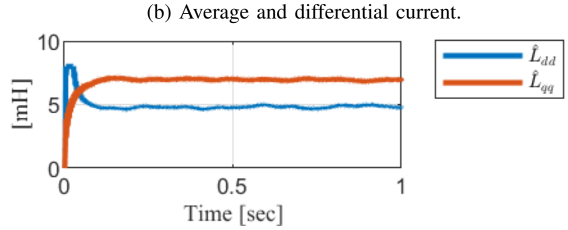

(c) Estimated dq incremental inductance.

Fig. 8: Real time inductance estimation result with operating condition, I_d = 10A, I_q = -15A at 200RPM, with V_{HFI} = 10V, f_{HFI} = 250Hz.

been used see Fig. 6. Finally, Fig. 8 (c) shows the estimated d and q-axes incremental inductance using (15) and (16) after saturation limit block in Fig. 6. As expected, d-axis incremental inductance is smaller than q-axis inductance since the machine is operating in the FI region (positive d-axis current).

Figure 9 shows experimental results changing dq-axes currents from -15A to 15A (i.e., -1p.u. to 1p.u.), currents being changed in steps of 5A, covering, therefore, operating conditions in the four quadrants of the dq current plane. Figure 9 (a) and Fig. 10 (a) show L_{dd}, experimental and the FEA respectively, while Fig. 9 (b) and Fig. 10 (b) show L_{qq}, experimental and the FEA respectively. The maximum estimation error in the dq-current plane is 14% for L_{dd} and 18% for L_{qq}. The maximum error occur in the maximum saturation operating point with 1p.u. of d-axis current and 1p.u. of q-axis current. The proposed technique estimate the inductance seen from the driver. It is shown that the d-axis HF inductance increases in the FW region while it decreases in the FI region, which was an expected result. Also, it is seen that the q-axis inductance is bigger than the d-axis inductance because the PM flux is biasing the d-axis flux path.

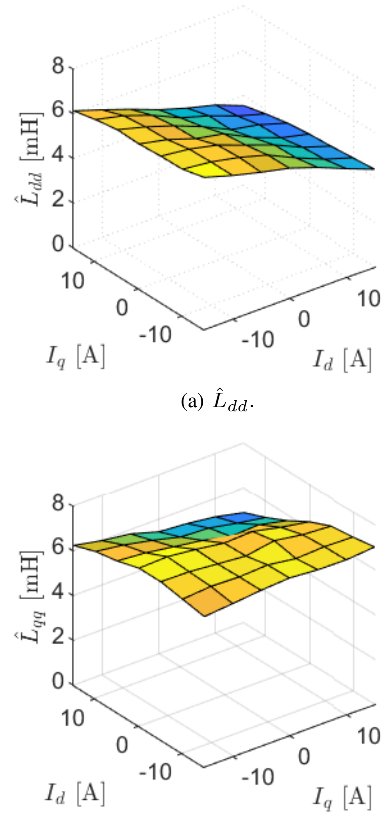

(a) $\hat{L}_{dd}$.

(b) $\hat{L}_{qq}$.

Fig. 9: Experimental results of dq-inductance map, 8-pole, 24-slot DW SPMSM.

B. Self-sensing performance monitoring on DW and FSCW SPMSMs

In this subsection, the self-sensing ability is monitored during FI and FW operation. For these experimental results, 8-pole, 12-slot SPMSM and 8-pole, 18-slot SPMSM are used. D-axis current in ±2p.u. is injected, and the dq-incremental inductance is estimated in both machines in real-time.

Figure 11 is showing the estimated inductance of both SPMSMs. The estimation result is compared with the estimation result using flux based inductance estimation in locked rotor position with square voltage injection [10]. The decreasing d-axis inductance with FI operation is due to superimposing saturation effect from both PM and d-axis current in FI operation. The inductive saliency, i.e.,, the gap between $\hat{L}_{dd}$ and $\hat{L}_{qq}$, increased in FI region and decreased in FW region.

Figure 12 shows the magnitude of decoupled average and differential HF current currents of both SPMSMs under test. It can be observed that in both SPMSMs, I_{i1}, which represents the self-sensing sensitivity, increased in the when flux-intensifying current is being injected, i.e., $+I_d$. On the contrary I_{i1} decreases when injecting flux-weakening current, i.e., -I_d. It can be concluded, therefore, that operating SPMSMs in FI direction enhances the saliency-based self-sensing using HFI, i.e., $+I_d$ would be the preferred option for self-sensing control.

V. Conclusions

This paper presents an on-line dq-incremental inductance estimation technique based on a HF injection with a fixed injection angle at $-45°$. By injecting HFI in between d and q-axes, the average and differential current are decoupled automatically, to estimate dq-incremental inductance. No machine parameters nor machine models are required using the proposed methodology. In addition, self-sensing sensitivity is monitored to find suitable operating conditions for inductive saliency-based self-sensing. Experimental results have been provided to demonstrate the feasibility of the proposed technique.

References

[1] Zhiqian Chen, M. Tomita, S. Doki, and S. Okuma, “An extended electromotive force model for sensorless control of interior permanent-magnet synchronous motors,” *IEEE Transactions on Industrial Electronics*, vol. 50, no. 2, pp. 288–295, April 2003.

[2] S. Morimoto, K. Kawamoto, M. Sanada, and Y. Takeda, “Sensorless control strategy for salient-pole PMSM based on extended emf in rotating reference frame,” *IEEE Transactions on Industry Applications*, vol. 38, no. 4, pp. 1054–1061, July 2002.

[3] P. L. Jansen and R. D. Lorenz, “Transducerless position and velocity estimation in induction and salient AC machines,” *IEEE Transactions on Industry Applications*, vol. 31, no. 2, pp. 240–247, March 1995.

[4] M. J. Corley and R. D. Lorenz, “Rotor position and velocity estimation for a salient-pole permanent magnet synchronous machine at standstill and high speeds,” *IEEE Transactions on Industry Applications*, vol. 34, no. 4, pp. 784–789, 1998.

[5] A. Yoo and S. Sul, “Design of flux observer robust to interior permanent-magnet synchronous motor flux variation,” *IEEE Transactions on Industry Applications*, vol. 45, no. 5, pp. 1670–1677, Sep. 2009.

[6] I. Boldea, M. C. Paicu, and G. Andreescu, “Active flux concept for motion-sensorless unified AC drives,” *IEEE Transactions on Power Electronics*, vol. 23, no. 5, pp. 2612–2618, Sep. 2008.

[7] D. Reigosa, Y. G. Kang, M. Martinez, D. Fernandez, J. M. Guerrero, and F. Briz, “SPMSMs sensorless torque estimation using high frequency signal injection,” *IEEE Transactions on Industry Applications*, pp. 1–1, 2020.

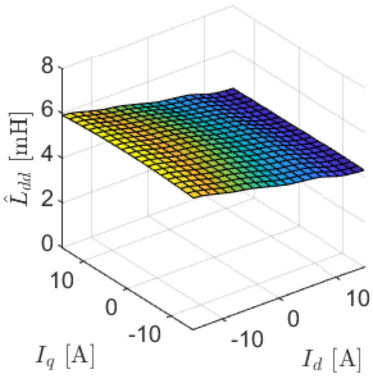

(a) $\hat{L}_{dd}$.

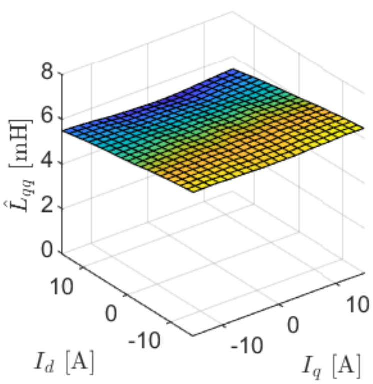

(b) $\hat{L}_{qq}$.

Fig. 10: FEA results of dq-inductance map, 8-pole, 24-slot DW SPMSM.

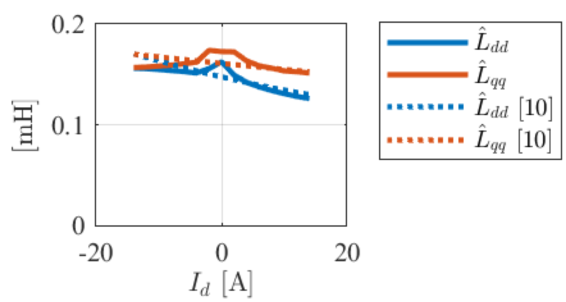

(a) $\hat{L}_{dd}$ and $\hat{L}_{qq}$, 8-pole, 12-slot DW-SPMSM.

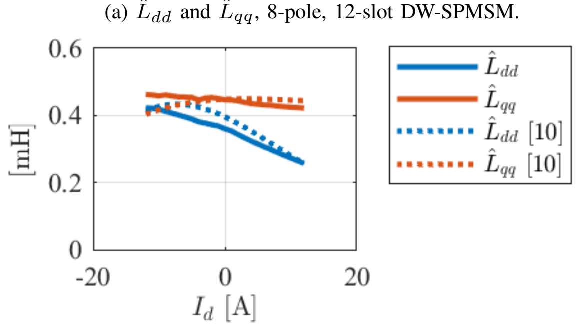

(b) $\hat{L}_{dd}$ and $\hat{L}_{qq}$, 8-pole, 18-slot CW-SPMSM.

Fig. 11: Inductance estimation comparison between the proposed method and [10] in FI and FW operating condition.

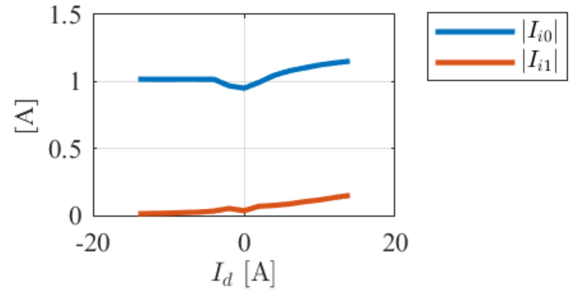

(a) I_{i0} and I_{i1}, 8-pole, 12-slot DW-SPMSM.

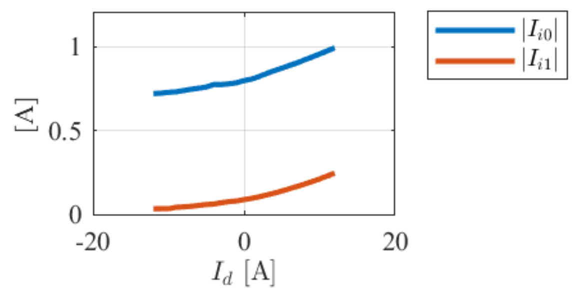

(b) I_{i0} and I_{i1}, 8-pole, 18-slot CW-SPMSM.

Fig. 12: Self-sensing ability monitoring on FI and FW operating condition with V_{HFI} = 2V, f_{HFI} = 1000Hz.

[8] H. Jung, D. Park, H. Kim, S. Sul, and D. J. Berry, "Non-invasive magnet temperature estimation of ipmsm based on high-frequency inductance with a pulsating high-frequency voltage signal injection," *IEEE Transactions on Industry Applications*, vol. 55, no. 3, pp. 3076–3086, 2019.

[9] D. Reigosa, D. Fernández, M. Martínez, J. M. Guerrero, A. B. Diez, and F. Briz, "Magnet temperature estimation in permanent magnet synchronous machines using the high frequency inductance," *IEEE Transactions on Industry Applications*, vol. 55, no. 3, pp. 2750–2757, 2019.

[10] B. Stumberger, G. Stumberger, D. Dolinar, A. Hamler, and M. Trlep, "Evaluation of saturation and cross-magnetization effects in interior permanent-magnet synchronous motor," *IEEE Transactions on Industry Applications*, vol. 39, no. 5, pp. 1264–1271, Sep. 2003.

[11] Q. Wang, G. Zhang, G. Wang, C. Li, and D. Xu, "Offline parameter self-learning method for general-purpose pmsm drives with estimation error compensation," *IEEE Transactions on Power Electronics*, vol. 34, no. 11, pp. 11 103–11 115, 2019.

[12] G. Stumberger, T. Marcic, B. Stumberger, and D. Dolinar, "Experimental method for determining magnetically nonlinear characteristics of electric machines with magnetically nonlinear and anisotropic iron core, damping windings, and permanent magnets," *IEEE Transactions on Magnetics*, vol. 44, no. 11, pp. 4341–4344, 2008.

[13] K. M. Rahman and S. Hiti, "Identification of machine parameters of a synchronous motor," in *38th IAS Annual Meeting on Conference Record of the Industry Applications Conference, 2003.*, vol. 1, 2003, pp. 409–415 vol.1.

[14] E. Armando, R. I. Bojoi, P. Guglielmi, G. Pellegrino, and M. Pastorelli, "Experimental identification of the magnetic model of synchronous machines," *IEEE Transactions on Industry Applications*, vol. 49, no. 5, pp. 2116–2125, 2013.

[15] M. Hinkkanen, P. Pescetto, E. Mölsä, S. E. Saarakkala, G. Pellegrino, and R. Bojoi, "Sensorless self-commissioning of synchronous reluctance motors at standstill without rotor locking," *IEEE Transactions on Industry Applications*, vol. 53, no. 3, pp. 2120–2129, 2017.

[16] X. Wu, X. Fu, M. Lin, and L. Jia, "Offline inductance identification of IPMSM with sequence-pulse injection," *IEEE Transactions on Industrial Informatics*, vol. 15, no. 11, pp. 6127–6135, 2019.

[17] N. Bedetti, S. Calligaro, and R. Petrella, "Stand-still self-identification of flux characteristics for synchronous reluctance machines using novel saturation approximating function and multiple linear regression," *IEEE Transactions on Industry Applications*, vol. 52, no. 4, pp. 3083–3092, 2016.

[18] S. A. Odhano, R. Bojoi, G. Roşu, and A. Tenconi, "Identification of

the magnetic model of permanent-magnet synchronous machines using dc-biased low-frequency AC signal injection," *IEEE Transactions on Industry Applications*, vol. 51, no. 4, pp. 3208–3215, 2015.

[19] Y. Shi, K. Sun, L. Huang, and Y. Li, "Online identification of permanent magnet flux based on extended kalman filter for IPMSM drive with position sensorless control," *IEEE Transactions on Industrial Electronics*, vol. 59, no. 11, pp. 4169–4178, 2012.

[20] S. M. Gadoue, D. Giaouris, and J. W. Finch, "MRAS sensorless vector control of an induction motor using new sliding-mode and fuzzy-logic adaptation mechanisms," *IEEE Transactions on Energy Conversion*, vol. 25, no. 2, pp. 394–402, 2010.

[21] T. Orlowska-Kowalska and M. Dybkowski, "Stator-current-based MRAS estimator for a wide range speed-sensorless induction-motor drive," *IEEE Transactions on Industrial Electronics*, vol. 57, no. 4, pp. 1296–1308, 2010.

[22] Hyunbae Kim and R. D. Lorenz, "Improved current regulators for IPM machine drives using on-line parameter estimation," in *Conference Record of the 2002 IEEE Industry Applications Conference. 37th IAS Annual Meeting (Cat. No.02CH37344)*, vol. 1, 2002, pp. 86–91 vol.1.

[23] M. Martinez, D. Reigosa, D. Fernández, J. M. Guerrero, and F. Briz, "Enhancement of permanent-magnet synchronous machines torque estimation using pulsating high-frequency current injection," *IEEE Transactions on Industry Applications*, vol. 56, no. 1, pp. 358–366, 2020.

[24] J. Zhou, K. Huang, S. Huang, S. Liu, H. Zhao, and M. Shen, "Inductance parameter identification method of permanent magnet synchronous motor based on the hf rotating square wave voltage injection," in *2019 22nd International Conference on Electrical Machines and Systems (ICEMS)*, 2019, pp. 1–4.

[25] W. Xu and R. D. Lorenz, "High-frequency injection-based stator flux linkage and torque estimation for DB-DTFC implementation on IPMSMs considering cross-saturation effects," *IEEE Transactions on Industry Applications*, vol. 50, no. 6, pp. 3805–3815, 2014.

[26] G. El-Murr, D. Giaouris, and J. W. Finch, "Online cross-coupling and self incremental inductances determination of salient permanent magnet synchronous machines," in *5th IET International Conference on Power Electronics, Machines and Drives (PEMD 2010)*, 2010, pp. 1–4.

[27] Y. Lee, Y.-C. Kwon, S.-K. Sul, N. A. Baloch, and S. Morimoto, "Compensation of position estimation error for precise position-sensorless control of IPMSM based on high-frequency pulsating voltage injection," in *2017 IEEE Energy Conversion Congress and Exposition (ECCE)*. IEEE, 2017, pp. 859–864.

[28] Y.-C. Kwon, J. Lee, and S.-K. Sul, "Full torque-range low-speed sensorless drive for heavily saturated IPMSMs by manipulation of convergence point," in *2017 IEEE Energy Conversion Congress and Exposition (ECCE)*. IEEE, 2017, pp. 865–872.

[29] D. D. Reigosa, D. Fernandez, H. Yoshida, T. Kato, and F. Briz, "Permanent-magnet temperature estimation in pmsms using pulsating high-frequency current injection," *IEEE Transactions on Industry Applications*, vol. 51, no. 4, pp. 3159–3168, 2015.

[30] Y. g. Kang and R. D. Lorenz, "Using intentional magnetic saturation for hfi based self-sensing with SPMSMs," in *2018 IEEE International Conference on Power Electronics, Drives and Energy Systems (PEDES)*, Dec 2018, pp. 1–6.

[31] N. Bianchi, E. Fornasiero, and S. Bolognani, "Effect of stator and rotor saturation on sensorless rotor position detection," *IEEE Transactions on Industry Applications*, vol. 49, no. 3, pp. 1333–1342, 2013.

[32] D. Diaz Reigosa, P. Garcia, D. Raca, F. Briz, and R. D. Lorenz, "Measurement and adaptive decoupling of cross-saturation effects and secondary saliencies in sensorless controlled IPM synchronous machines," *IEEE Transactions on Industry Applications*, vol. 44, no. 6, pp. 1758–1767, 2008.

[33] Z. Chen, X. Cai, R. Kennel, and F. Wang, "Enhanced sensorless control of SPMSM based on stationary reference frame high-frequency pulsating signal injection," in *2016 IEEE 8th International Power Electronics and Motion Control Conference (IPEMC-ECCE Asia)*. IEEE, 2016, pp. 885–890.

[34] M. Cirrincione and M. Pucci, "An MRAS-based sensorless high-performance induction motor drive with a predictive adaptive model," *IEEE Transactions on Industrial Electronics*, vol. 52, no. 2, pp. 532–551, April 2005.

[35] Y. G. Kang, B. Sarlioglu, and R. D. Lorenz, "Saliency based self-sensing enhanced operating condition monitoring using high-frequency injection under intentional magnetic saturation," in *2019 IEEE International Electric Machines Drives Conference (IEMDC)*, 2019, pp. 922–927.

[36] T. W. Nehl, F. A. Fouad, and N. A. Demerdash, "Determination of saturated values of rotating machinery incremental and apparent inductances by an energy perturbation method," *IEEE Transactions on Power Apparatus and Systems*, vol. PAS-101, no. 12, pp. 4441–4451, Dec 1982.

[37] J. Arellano-Padilla, M. Sumner, C. Gerada, and G. Asher, "Prediction of inductance characteristics of PMSMs in saliency-based sensorless control," in *2012 15th International Power Electronics and Motion Control Conference (EPE/PEMC)*. IEEE, 2012, pp. LS3a–1.

Ye gu Kang received the B.S. degree in electrical engineering from Penn State University, University Park, PA, USA, in 2011, the M.S. degree in electrical engineering and the Ph.D. degree in mechanical engineering from the University of Wisconsin–Madison, Madison, WI, USA, in 2013 and 2019, respectively.,He is currently an Investigator with the University of Oviedo, Gijón, Spain. His research interests include the design and control of energy conversion devices.

David Reigosa was born in Spain 1979. He received the M.E. and PhD degrees in electrical engineering from the University of Oviedo, in 2003 and 2007, respectively. He is currently and Associated Professor in the Electrical Engineering Department, University of Oviedo. From 2004 to 2008, he was awarded and fellowship of the Personnel Research Training Program funded by Regional Ministry of Education and Science of the Principality of Asturias. He was a visitor scholar at the Wisconsin Electric Machines and Power Electronics Consortium, University of Wisconsin, Madison, in 2007. He was a visitor professor at the University of Sheffield (UK), Electrical Machines and Drives Group, in 2016. He was the recipient of nine IEEE Industry Applications Society Conference and IEEE Energy Conversion Congress and Exposition prize paper awards. His research interests include sensorless control of induction motors, permanent magnet synchronous motors and digital signal processing Biography text here.

Bulent Sarlioglu received the B.S. degree from Istanbul Technical University, Istanbul, Turkey, in 1990, the M.S. degree from the University of Missouri, Columbia, MO, USA, in 1992, and the Ph.D. degree from the University of WisconsinMadison, Madison,WI, USA, in 1999, all in electrical engineering. Since 2011, he has been a Professor with the University of Wisconsin-Madison and the Associate Director with the Wisconsin Electric Machines and Power Electronics Consortium. From 2000 to 2011, he was with Honeywell International Inc.'s Aerospace Division, Torrance, CA, USA, most recently as a Staff Systems Engineer. He has authored or coauthored more than 150 technical papers that are published in conference proceedings and journals. His research interests include electrical machines, drives, and power electronics, and he is the Inventor or Co-Inventor of 19 U.S. patents as well as many international patents. Dr. Sarlioglu was the recipient of Honeywell's Outstanding Engineer Award in 2011, NSF CAREER Award in 2016, and the fourth Grand Nagamori Award from Nagamori Foundation, Japan in 2019.

Robert D. Lorenz , deceased, received the B.S.M.E. and M.S.M.E.-Controls degrees from the University of Wisconsin-Madison, Madison, WI, USA, in 1969 and 1970, respectively, the M.B.A. degree from the University of Rochester, Rochester, NY, USA, in 1980, and the Ph.D. M.E.-Controls degree from the University of Wisconsin-Madison, in 1984.,From 1984, he was a Faculty Member with the Department of Mechanical Engineering, University of Wisconsin-Madison and an Associate Director of the Wisconsin Electric Machines and Power Electronics Consortium (WEMPEC). From 1997 to 2019, he was the Co-Director of WEMPEC. Prior to joining the university, he was with the industry for 12 years, working on high-performance drives and synchronized motion control. He has authored more than 400 technical papers and has more than 45 patent awards and applications in his research topics. His research interests include power electronics, drives, self-sensing, current regulators, and motion control.,Dr. Lorenz was the recipient of several awards from the IEEE Industry Applications Society and the European Power Electronics Associations, the 2014 IEEE Richard H. Kaufman Technical Field Award, and 33 IEEE Prize Paper Awards. He was the IEEE Division II Director during 2005–2006, IEEE IAS President in 2001, and a Distinguished Lecturer of IAS during 2000–2001. He was posthumously elected to the U.S. National Academy of Engineering in 2019.